Groundwater for Sustainable Development 20 (2023) 100886

Contents lists available at ScienceDirect

Groundwater for Sustainable Development

journal homepage: www.elsevier.com/locate/gsd

Research paper

Radon-rich waters of the Tulinka aquifers, Novosibirsk, Russia

D.A. Novikov [a,b], YuG. Kopylova [c], A.N. Pyryaev [d], A.A. Maksimova [b], A.S. Derkachev [b], A.F. Sukhorukova [a], F.F. Dultsev [a,b,*], A.V. Chernykh [a,b], A.A. Khvashchevskaya [c], P.N. Kalinkin [b], A.V. Petrozhitsky [e]

[a] A.A. Trofimuk Institute of Petroleum Geology and Geophysics, Siberian Branch, Russian Academy of Sciences, 3 Akademik Koptyug Ave., Novosibirsk, 630090, Russia
[b] Novosibirsk State University, 1, Pirogov Str., Novosibirsk, 630090, Russia
[c] Tomsk National Research Technological University, 30 Lenin Ave, Tomsk, 634050. Russia
[d] V.S. Sobolev Institute of Geology and Mineralogy, Siberian Branch, Russian Academy of Sciences, 3, Koptyug Ave., Novosibirsk, 630090, Russia
[e] G.I. Budker Institute of Nuclear Physics, Siberian Branch, Russian Academy of Sciences, 11, Akademik Lavrentiev Ave., Novosibirsk, 630090, Russia

HIGHLIGHTS

- Composition signatures of Tulinka radon waters reveal their origin and recharge characteristics.
- The origin of radon waters is meteoric, with minor contribution from deep waters.
- The radon waters recharge by infiltration of atmospheric precipitation.

GRAPHICAL ABSTRACT

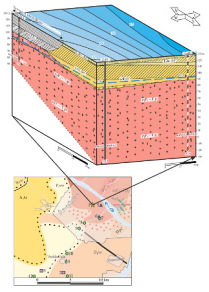

ARTICLE INFO

Keywords:
Groundwater
Radon
Stable isotopes
Radiocarbon age
Uranium
Thorium

ABSTRACT

The first integrated isotope and chemical data on radon-rich waters of the Tulinka aquifers (Novosibirsk, West Siberia) are presented. The Tulinka radon waters are fresh, with neutral to moderately alkaline pH (7.3–7.7), SO_4–HCO_3 Na–Mg–Ca major-ion chemistry. The amount of total dissolved solids is 720–910 mg/L, Si content 6.41–9.02 mg/L. Eh is within +169.1 – +250.0 mV, corresponding to oxidized conditions. The concentration of dissolved oxygen is 2.86–7.37 mg/L. Radon activity (^{222}Rn) varies from 173 to 276 Bq/L. The concentrations of U, Th, and Ra isotopes are 0.015–0.017 mg/L ^{238}U, $9.59 \bullet 10^{-7}$ to $1.58 \bullet 10^{-5}$ ^{232}Th, and up to $4.93 \bullet 10^{-10}$ ^{226}Ra; the ^{232}Th/^{238}U ratio is in the range $5.81 \bullet 10^{-5}$ to $9.42 \bullet 10^{-4}$. Total α activity is not higher than 891 mBq/L, and β activity is 80 mBq/L. The compositions of stable isotopes are −15.4 to −15.1‰ δ^{18}O, −114.2 to −112.8‰ δD, and −13.9 to −9.9‰ δ^{13}C. The isotope signatures and recharge patterns of the Tulinka waters are insensitive to seasonal effects, which suggests the slow water exchange. Substantial seasonal variations of the content of dissolved inorganic carbon (DIC) are detected. The range of $\delta^{13}C_{DIC}$ in the analyzed samples (from −14.3 to −9.0‰) corresponds to a mixed CO_2 origin: diffusion of soil CO_2 approaching the atmospheric $\delta^{13}C_{CO2}$ values, and biogenic CO_2 released by decaying plant residues. The measured isotope characteristics provide evidence that the waters recharge by infiltration from meteoric sources. The approximate radiocarbon age of DIC in the Tulinka

* Corresponding author. A.A. Trofimuk Institute of Petroleum Geology and Geophysics, Siberian Branch, Russian Academy of Sciences, 3Akademik Koptyug Ave., Novosibirsk, 630090, Russia.
E-mail address: Dultsevff@ipgg.sbras.ru (F.F. Dultsev).

https://doi.org/10.1016/j.gsd.2022.100886
Received 20 May 2022; Received in revised form 8 December 2022; Accepted 8 December 2022
Available online 10 December 2022

waters, determined for the first time, is 2663 ± 144 years. However, this age may be underestimated due to groundwater mixing with the present-day surface waters.

1. Introduction

Radon-rich waters are under extensive investigation due to their diversity in terms of chemistry, isotope systematics, age, and aquifer settings (Duenas et al., 1998; Horvath et al., 2000; Bohm, 2002; Bertolo and Bigliotto, 2004; Beitollahi et al., 2007; Gurler et al., 2010; Song et al., 2011; Roba et al., 2012; Nikolov et al., 2012; Atkins et al., 2016; Mittal et al., 2016; Seminsky et al., 2017; Abu-Khader et al., 2018; Telahigue et al., 2018; Poojitha et al., 2020 et al.). Radon (^{222}Rn) is a radioactive inert gas, a progeny of ^{238}U. According to WHO, this gas is the most frequent source of natural radioactivity, responsible for up to 98% of the average yearly effective doses of radiation, thus contributing into risks to human health. On the other hand, radon is broadly used in balneotherapy.

This study is a continuation of our previous work (Novikov et al., 2018,2020a; Novikov and Korneeva, 2019; etc.) on the formation mechanisms and chemistry of radon waters in the Novosibirsk urban area, where the groundwaters are enriched with radon due to the features of local geology: about 70% of the area is occupied by the shallow-bedded Novosibirsk granite complex, which supplies radioactive elements to aquifers. Previous geological surveys within the Novosibirsk complex and its surroundings revealed more than ten occurrences of radon-rich waters: Zaeltsovskoye, Kamenka, Tulinka, etc. The Tulinka radon waters have been used at a spa of City Clinics 34, the only radon spa site that continues functioning (Fig. 1).

The radon waters of the Novosibirsk urban area remain poorly investigated. The goal of our work is to provide integrated characterization of radon-rich Tulinka waters, with further outlooks to ensure improvement of their effective and sustainable management with the possibility to evaluate their spa potential and health risks. The present work is the first communication to bridge the gap by presenting the first integrated data on the Tulinka waters, including major-ion chemistry, total ά and β activity, ^{222}Rn activity, radiocarbon age (^{14}C), and isotope systematics (δD, δ^{18}O, δ^{13}C, ^{234}U, ^{238}U, ^{226}Ra, and ^{228}Ra).

2. Methods and measurements

The isotope systematics and major-ion chemistry were analyzed in natural waters sampled from the left bank of the Ob River within the Novosibirsk urban area during the field works in 2019–2020. The chemistry of the radon-rich groundwaters of Tulinka aquifers was monitored continuously from May 2019 through March 2020, except for July 2019 and April 2020, when monitoring was interrupted for technical reasons.

The variables (pH, Eh, temperature, and dissolved O_2 and HCO_3^-) were measured under the field conditions directly on the sampling site, using the instruments of the field laboratory (*Hanna HI9125* and *AKPM-1-02L* oxygen meter). Radon in natural waters was measured with the help of an *AlfaradPlus* system (measurement error did not exceed 5%) at the Laboratory for Basin Hydrogeology in the A.A. Trofimuk Institute of Petroleum Geology and Geophysics (Novosibirsk, West Siberia, Russia). The water chemistry was analyzed using titration, ion chromatography, and mass spectrometry with inductively coupled plasma at the Water Chemistry Laboratory of the Engineering School for Natural Resources at the Tomsk National Research Polytechnical University.

Results of the analysis of ion composition of waters have been subjected to intra-laboratory quality control with respect to consistency between the total concentrations of anions and cations, which are to differ from each other by not more than 10% according to the requirements of the Scientific Board on Analytical Methods to hydrogeochemical studies (SCAM, 1987). In cases if corrections are necessary, they are carried out within the error limits of specific parameters in agreement with the normative document of measurement procedure.

Titration was used to determine hydrocarbonate ions: 50 mL of water sample under investigation was titrated with 0.1 N solution of hydrochloric acid to obtain pH 4.3. Measurement error does not exceed 20%. Determination of the concentrations of calcium, magnesium, sodium, potassium cations, sulfate, chloride and nitrate anions was carried out by means of ion chromatography using a Dionex ICS-5000 chromatograph (Dionex, USA). Measurement error did not exceed 15% within the concentration range of 0.05–1000 mg/L.

The elemental composition of water was determined by means of mass spectrometry with inductively coupled plasma using a NexION 300D mass spectrometer (PerkinElmer, USA) with a background suppression cell UCT in the standard collision mode, with helium as carrier gas. The range of the measured element concentrations was 0.05–10000 μg/L. The element detection limit was not more than 11 ng/L with respect to beryllium (^{9}Be). Indium was added as the internal standard to

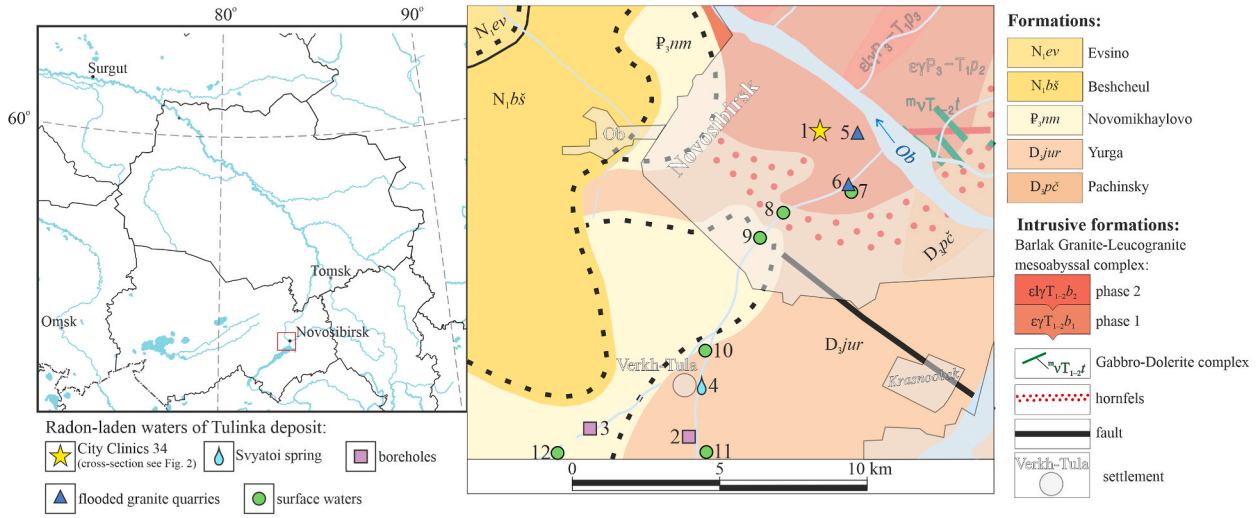

Fig. 1. Location map and sampling sites.

provide control of the sensitivity of mass spectrometer. Element content in the samples under investigation was calculated taking into account detection limits and included calculations of the true element concentrations on the basis of results obtained through analyses of calibration solutions. The accuracy of analysis was checked using multi-element calibration standard solutions (PerkinElmer, USA).

Stable isotopes of oxygen ($\delta^{18}O$), deuterium (δD), and carbon ($\delta^{13}C_{DIC}$) were determined at the Analytical Center of the V.S. Sobolev Institute of Geology and Mineralogy (Novosibirsk), on a *Finnigan^{TM} MAT 253* Isotope Ratio Mass Spectrometer, equipped with a sample preconditioning H/Device (for δD) and a GasBench II system (for $\delta^{18}O$ and $\delta^{13}C_{DIC}$). The measurements were performed according to conventional procedures (Epstein and Mayeda, 1953; Nelson, 2000; Evans et al., 2008; Kopec et al., 2019), relative to the standards of the International Atomic Energy Agency (IAEA): VSMOW2, SLAP2, and GISP for δD and $\delta^{18}O$; NBS-18 and NBS-19 for $\delta^{13}C_{DIC}$. The measurement accuracy was 0.1‰ for $\delta^{18}O$ and $\delta^{13}C_{DIC}$, and 2‰ for δD.

The total α and β activity of natural waters, as well as the activities of ^{234}U, ^{238}U, ^{226}Ra and ^{228}Ra isotopes, were measured after radioactive preconditioning using several instruments: ALPHA-ENSEMBLE-8 alpha spectrometer (Ametek, ORTEC, USA); gamma spectrometry system based on a well-type coaxial HPGe detector with the Eurisys Measures low background cryostate EGPC 192-P21/SHF 00-30 A-CLF-FA (France), and UMF-2000 alpha-beta radiometer with a *Dosa* silicon detector for low-activity measurements (measurement error did not exceed 5%). Radiocarbon ($\delta^{14}C$) ages of natural waters were determined using an accelerating mass spectrometer at the Analytical Center of the G.I. Budker Institute of Nuclear Physics (Novosibirsk). The quality characteristics of the Tulinka radon waters were evaluated according to the State Standard (2020).

The Tulinka aquifers of radon-rich groundwaters is located in the Lenin district of Novosibirsk, within the area of City Clinics 34 (No. 18, Titov Street). The history of the spa began in 1978, when a team from the Vostokburvod Company drilled a 70 m long test borehole (BH 100e). Two more boreholes were drilled in 1985 (151.4 and 151.5 m deep, boreholes 1–44 and 2–45, respectively) in response to increasing demand for therapeutic radon waters, which reached 150 m^3/day. Test and experimental water withdrawal from the boreholes was performed in 1986–1987 by the Novosibirsk Geological Survey. The results of tests were used to estimate the radon water resources of C_1 category at the Tulinka aquifers, which amounted to 207 m^3/day. Currently borehole No. 10–213 is the only operating borehole for radon water withdrawn from the depth of 70 m.

3. Hydrogeological setting

The Tulinka radon water occurrence is located in the Trans-Ob Plain which has a rough surface with the incised Ob River valley and its terrace III, at elevations of 135–140 m. There are two main aquifers within the Novosibirsk granite intrusion ($\varepsilon\gamma P_3 - T_1p_2$) buried under Cenozoic sediments (Fig. 2). The upper aquifer consists of pore waters in Quaternary sediments (Holocene (a_3Q_{IV}) alluvium and the Krasnaya Dubrovka (L,laI-IIkd) and Kochkovo (a,lE$_2$kč) Formations), and the lower aquifer comprises interstitial waters in sheared granitoids, the main phase of the Novosibirsk complex (Babin et al., 2015). The rocks of the upper aquifer include silt, clay silt, and fine sand varying in total thickness from 28 to 43.8 m. The waters of the lower aquifer are hosted by sheared yellowish-grayish medium-grained biotite-hornblende porphyry granites. The granitic rocks have been cored till the maximum depth of borehole 2–45 (111.5 m). The rocks are cut by two fracture

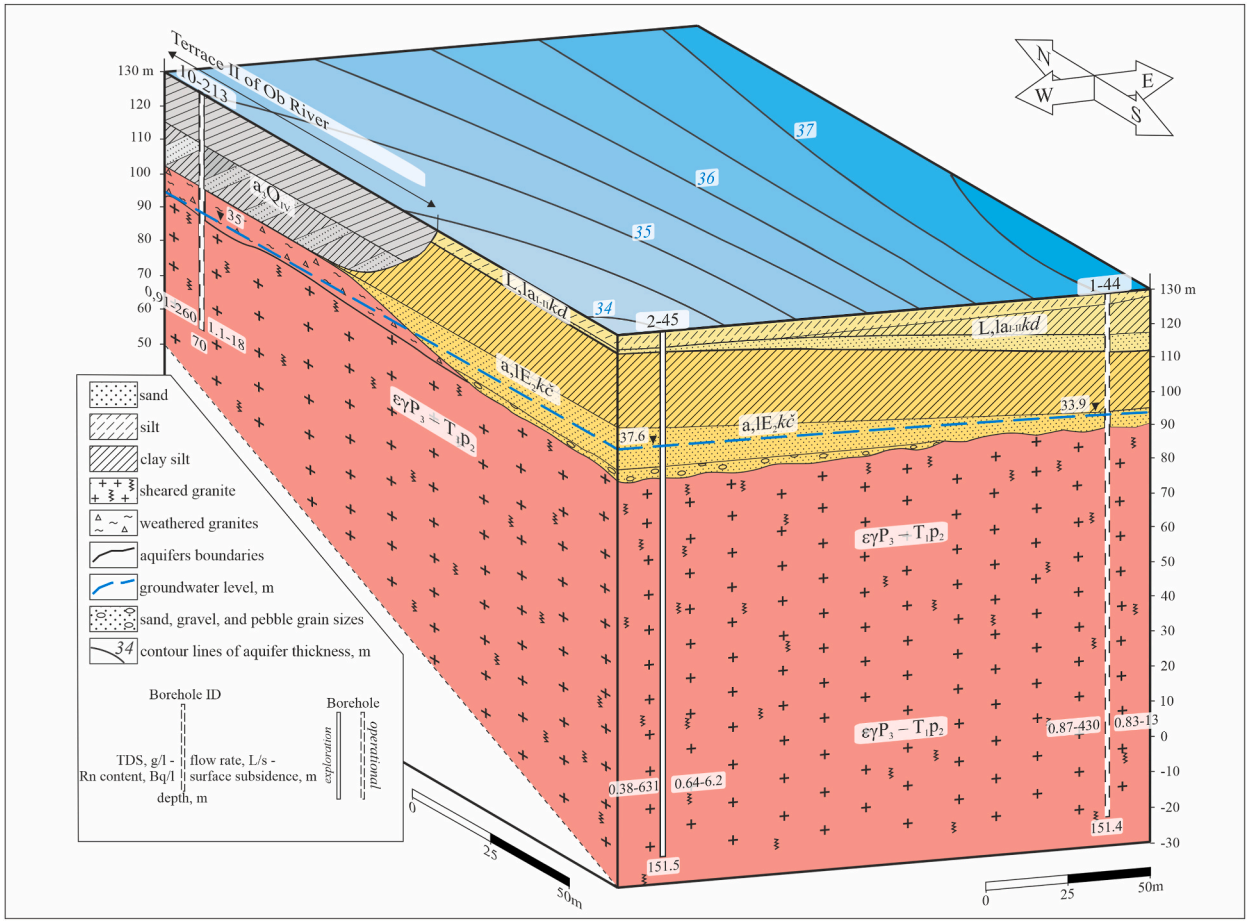

Fig. 2. Block structure of aquifers at Tulinka territory (by the example of City Clinics 34).

systems oriented at 20–30° and 50–60°, respectively, relative to the core axis. The density of fractures increases upward, from monolith granites at a depth of 70 m in borehole 10–213 to 9 m of pebble-to clay-size eluvium 28 m below the surface, found locally in the northwestern part of the occurrence. The aquifers are hydraulically connected, as evidenced by the existence of a single piezometric surface revealed in the 33.9–37.6 m depth interval of the boreholes. Water content is non-uniformly distributed over the occurrence, and the flow rates of boreholes vary from 0.06 to 0.13 L/s.

4. Results and discussion

4.1. Major-ion chemistry

The radon-rich waters of the Tulinka aquifers (Table 1) are characterized by the SO_4–HCO_3 Na–Mg–Ca major-ion chemistry (Fig. 3), with total salinity (TDS) 720–910 mg/L and Si content 6.41–9.02 mg/L. The variables, namely pH, Eh and the concentration of dissolved O_2, are mainly controlled by local geology and water exchange patterns. The Tulinka waters have neutral to slightly alkaline pH (7.3–7.7) and Eh values from +169.1 to +250.0 mV, corresponding to the oxidized environment, and contain 2.86–7.37 mg/L of dissolved oxygen.

According to the values of average element ratios Ca/Na = 3.5, Ca/Mg = 3.3, Ca/Si = 16.1, Mg/Si = 5.0, Na/Si = 4.7, Si/Na = 0.2, rNa/rCl = 1.4, and SO_4/Cl = 2.0, these are interstitial waters in sheared granitoids (group I). High nitrate concentration within the range of 30.0–59.3 mg/L shows that the producing aquifer is subject to initial anthropogenic pollution caused by flooding of the Quaternary sediments and the fractured granites. The same process was revealed at the Kamenka occurrence located on the right bank of the Ob River in the Novosibirsk Urban Area (Novikov et al., 2021a). The isotope and chemical data for the Tulinka aquifers exposed to flooding were compared with those for other water groups of the area (Fig. 3): interstitial waters of the regional fractured zone, from a spring and two boreholes in Verkh Tula village (group II), surface waters in flooded granite quarries of Gorsky and Tulinka under anthropogenic impact (group III), and in the Upper Tula and Tula rivers (group IV).

The group II waters sampled in Verkh Tula village are of two main types: (i) background waters from the Svyatoi spring (2 and 4 in Fig. 1), and a borehole (2 in Fig. 1); (ii) polluted waters from another borehole (3 in Fig. 1). The background waters are of HCO_3 Na–Mg–Ca chemical type, with total salinity of 587–731 mg/L and 4.1–7.0 mg/L silica, pH is within 7.4–7.6; Eh corresponds to the reduced environment (−27.8 to −157.4 mV), and dissolved oxygen varies from 0.3 to 2.1 mg/L. Compared to the Tulinka waters, the background waters of group II have higher ratios of Mg/Si (6.3), Na/Si (6.0), rNa/rCl (16.4), and SO_4/Cl (4.4), lower ratios of Ca/Na (2.6), Ca/Mg (2.6), and Ca/Si (15.5), and the same Si/Na ratio equal to 0.2. This composition indicates that Na and Mg cations were accumulated under similar conditions by water interaction with mainly aluminosilicate clastic rocks. Water from the other borehole in Verkh Tula village (3 in Fig. 1) has positive Eh value, +81.8 mV, with up to 5.5 mg/L O_{2aq}, corresponding to oxidized conditions, and bears signatures of anthropogenic pollution, which is confirmed by the high concentrations of Ni, Zn (up to 0.019 mg/L each), Cu (0.0044 mg/L), Hg ($2.3\bullet10^{-5}$ mg/L), etc.

The quarry surface waters (group III) exposed to anthropogenic effects belong to the Cl–SO_4–HCO_3 Na–Mg–Ca type, their total salinity is 403–541 mg/L, and contain from 0.25 to 0.78 mg/L SiO_2 (Table 1). They are characterized by alkaline pH (8.5–8.7), positive Eh (+131.3 to +250.0 mV), and $O_{2\ aq}$ contents of 6.9–11.3 mg/L. The corresponding average element ratios are Ca/Na = 1.5, Ca/Mg = 1.7, Ca/Si = 121.6, Mg/Si = 71.4, Na/Si = 88.9, Si/Na = 0.01, rNa/rCl = 1.5 and SO_4/Cl = 1.4.

The river surface waters (group IV), likely exposed to anthropogenic effects, have SO_4–HCO_3 Na–Mg–Ca chemistry and 542–713 mg/L salinity, and differ from the waters of group III in higher Si content (0.5–3.7 mg/L), lower pH (7.9–8.2), and slightly higher positive Eh (+210.0 to +260.5 mV), with 1.7–11.4 mg/L O_{2aq}. The difference is also in higher element ratios reaching Ca/Mg = 3.2, Si/Na = 0.05, rNa/rCl = 3.9, and SO_4/Cl = 3.5, with the lower ratios of Ca/Si (55.4), Mg/Si (22.3), and Na/Si (36.0). The reason may be that the river network drains the aquifer, which is evidenced by high silica (3.7 mg/L) and lithium (0.0076 mg/L).

Analyses of minor and trace elements in the Tulinka waters show accumulation of Fe, Zn, Mn, Cu, Ti, Sc, Ni, Co, and Y, with general salinity increase. The highest contents were measured for Si (9.02), Sr (0.92), B (0.47), Fe (0.31), I (0.24), Br (0.22), Ba (0.06), U (0.02), Li (0.02), while other elements occur in low concentrations: $2.0\bullet10^{-6}$ Al, $1.8\bullet10^{-6}$ Zn, $9.5\bullet10^{-7}$ Ga, $2.4\bullet10^{-6}$ Ge, $2.0\bullet10^{-6}$ Y, $2.1\bullet10^{-7}$ Pd, $1.5\bullet10^{-7}$ Sn, $3.1\bullet10^{-7}$ Hf, and $9.6\bullet10^{-7}$ Th (Fig. 4a).

The accumulation of elements in the radon-rich Tulinka waters was estimated *via* enrichment factors, that is, the ratios of element contents in water to those in the host rocks or in the average upper continental crust. Enrichment factors (Fig. 4b) are the highest for I (0.13), Br (0.05), Se (0.03), B (0.03), and Te (0.01), and correlate with the mobility of elements (Fig. 4c). The mobility is very high for I (159,6), Br (59.1), Se (40.2), B (13.1), and Te (12.1); high for U (7.9) and Sr (3.8); medium for Li (0.55), Mo (0.52), Pd (0.24), Sb (0.34), and Ba (0.11); and low for most of elements: As (0.089), P (0.070), Sc (0.051), W (0.049), Cs (0.044), Cr (0.041), Si (0.034), Sn (0.034), Zn (0.032), Cu (0.031), Rb (0.019), Ni (0.016), Pb (0.013), Co (0.005), Fe (0.004), V (0.004), Ge (0.004), Mn (0.002), Zr (0.001), Hf (0.0006), Th (0.0006), Y (0.0004), Ti (0.0002), Ga (0.0002), and Al ($2.2\bullet10^{-5}$).

4.2. Radionuclides

The contents of radioactive elements in natural waters are of key importance, especially for mineral water occurrences. ^{222}Rn activity in the Tulinka waters varies from 173 to 276 Bq/L, which corresponds to very low- or low-radon waters in the classification of Tolstikhin (Posokhov and Tolstikhin, 1977). The total α and β activity levels do not exceed 891 mBq/L and 80 mBq/L, respectively. Natural radionuclides are 0.015–0.017 mg/L ^{238}U and $4.93\bullet10^{-10}$ mg/L ^{226}Ra (Table 2). The concentrations of thorium, analyzed for the first time in the groundwater of Tulinka aquifers, vary from $9.59\bullet10^{-7}$ to $1.58\bullet10^{-5}$ mg/L ^{232}Th. Since the times of V. Vernadsky (1920s–1930s), the concentrations of Th and its progenies in water have been considered to be below detection limits. Vernadsky considered thorium to be beyond water chemistry and beyond the Earth's water budget. In our case, the ^{232}Th/^{238}U ratio is within the range expectable for oxidized environments: $5.81\bullet10^{-5}$ to $9.42\bullet10^{-4}$. The activities of U and Ra isotopes in the Tulinka waters are 706 mBq/L for ^{234}U, 196 mBq/L for ^{238}U, 18 mBq/L for ^{226}Ra, and 20 mBq/L for ^{228}Ra, and the isotope ratio ^{234}U/^{238}U (γ) is within 3.6. This confirms the previous hypothesis of their mixing with the waters of the flooded zone.

For comparison, ^{222}Rn in the waters of background composition (Svyatoi spring in Verkh Tula village) ranges from 7 to 28 Bq/L. The total activity α is 327 mBq/L, and β activity is 20 mBq/L. Other radionuclides are 0.005–0.007 mg/L ^{238}U, $3.01\bullet10^{-7}$ to $8.00\bullet10^{-6}$ mg/L ^{232}Th, and $2.46\bullet10^{-10}$ mg/L ^{226}Ra. The ^{232}Th/^{238}U ratio ranges from $6.38\bullet10^{-5}$ to $4.29\bullet10^{-3}$. Note that the ^{238}U and ^{232}Th concentrations in the waters from the boreholes in Verkh Tula village are lower than in the spring ($3.80\bullet10^{-6}$ and $8.00\bullet10^{-6}$ mg/L, respectively), while the ^{232}Th/^{238}U ratio reaches 1.84 to 2.96. The activity values of U and Ra isotopes in the Svyatoi spring are 147 mBq/L ^{234}U, 115 mBq/L ^{238}U, 9 mBq/L ^{226}Ra, and 7 mBq/L ^{228}Ra; the ^{234}U/^{238}U ratio (γ) does not exceed 1.3, which means a minor contribution from deep waters, because the ^{234}U/^{238}U ratio is known to serve as an indirect indicator of the contribution from deep waters into an aquifer (Osmond and Rydell, 1968).

The analyzed waters mainly occur in oxidized conditions, and uranium has the highest mobility. Its distribution correlates with water

Table 1
Major-ion chemistry and properties of the Tulinka radon-laden waters.

		No in Fig. 1	Sampling date	pH	Eh, mV	^{222}Rn, Bq/L	O_2, mg/L	PI*	Elements, mg/L									TDS, mg/L	Chemical type**
									Ca^{2+}	Mg^{2+}	Na^{+}	K^{+}	HCO_3^-	SO_4^{2-}	Cl^-	NO_3^-	Si		
Interstitial waters in sheared granitoids (group I)		1	May 13, 2019	7.8	+191.0	–	6.0	0.7	141	40.5	36.8	2.4	537	67.0	32.1	53.0	8.6	910	SO_4–HCO_3 Na–Mg–Ca
		1	May 30, 2019	7.5	+250.0	173	3.5	1.4	112	45.8	56.1	2.2	586	52.0	36.0	30.0	6.4	890	HCO_3 Na–Mg–Ca
		1	June 27, 2019	7.5	+169.1	218	2.9	0.1	148	33.5	32.7	2.2	530	54.0	28.0	57.0	6.8	828	SO_4–HCO_3 Na–Mg–Ca
		1	August 01, 2019	7.4	+192.6	–	4.1	1.0	112	39.0	35.1	2.2	460	96.0	29.9	48.9	8.1	774	SO_4–HCO_3 Na–Mg–Ca
		1	September 03, 2019	7.6	+231.1	247	6.8	0.6	108	31.0	31.1	2.1	482	47.4	18.0	52.6	7.7	720	SO_4–HCO_3 Na–Mg–Ca
		1	October 09, 2019	7.5	+197.8	–	6.6	0.1	148	33.5	32.7	2.2	530	54.0	28.0	57.0	6.5	828	SO_4–HCO_3 Na–Mg–Ca
		1	November 12, 2019	7.6	+197.6	218	7.4	0.3	121	37.8	31.4	2.1	561	24.5	28.7	48.2	7.5	807	HCO_3 Na–Mg–Ca
		1	December 11, 2019	7.6	+190.7	217	7.2	–	115	40.0	32.2	2.4	522	57.3	29.0	59.2	8.2	799	SO_4–HCO_3 Na–Mg–Ca
		1	January 21, 2020	7.6	+212.8	–	6.9	–	130	36.6	34.0	2.1	500	61.0	29.0	59.3	8.3	852	SO_4–HCO_3 Na–Mg–Ca
		1	February 12, 2020	7.6	+193.9	–	6.0	0.4	101	42.3	28.0	2.2	393	68.6	35.0	53.0	8.0	724	Cl–SO_4–HCO_3 Na–Mg–Ca
		1	March 18, 2020	7.6	+185.3	276	5.7	0.3	107	38.0	40.0	2.7	454	59.0	29.8	52.0	9.0	783	SO_4–HCO_3 Na–Mg–Ca
			Average:	**7.5**	**+201.1**	**225**	**5.7**	**0.5**	**122**	**40.0**	**35.5**	**2.3**	**505**	**58.2**	**24.4**	**52.0**	**7.7**	**811**	–
Interstitial waters in regional fractured zone (group II)		2	June 17, 2019	7.6	−157.4	6	0.3	1.8	76	45.0	45.0	1.2	535	19.7	9.6	1.3	6.5	731	HCO_3 Na–Mg–Ca
		3	June 17, 2019	7.7	+81.8	0	5.5	2.8	99	36.0	30.0	0.5	525	11.8	12.4	1.1	6.1	715	HCO_3 Na–Mg–Ca
		4	June 03, 2019	7.4	−44.8	28	0.5	1.7	80	42.0	32.0	1.1	512	11.9	7.2	1.5	4.1	686	HCO_3 Na–Mg–Ca
		4	June 27, 2019	7.5	−64.0	16	1.1	0.4	80	27.5	27.0	1.5	445	5.0	1.1	1.5	6.6	587	HCO_3 Na–Mg–Ca
		4	February 24, 2020	7.5	−27.8	–	2.1	1.4	96	36.5	30.2	1.4	520	20.0	5.4	1.9	4.3	714	HCO_3 Na–Mg–Ca
		4	June 23, 2020	7.5	−50.7	17	1.2	1.2	100	28.1	36.0	1.7	503	14.3	1.1	2.3	6.9	695	HCO_3 Na–Mg–Ca
		4	July 07, 2020	7.6	−55.2	11	2.0	2.4	90	28.1	34.2	1.5	470	7.5	6.8	1.7	7.0	650	HCO_3 Na–Mg–Ca
			Average:	**7.5**	**−45.4**	**13**	**1.8**	**1.7**	**88.7**	**34.7**	**33.5**	**1.3**	**501.4**	**12.9**	**6.2**	**1.6**	**5.9**	**683**	–
Surface water subject to anthropogenic effects	quarries (group III)	5	May 12, 2019	8.7	+250.0	0	6.9	2.4	48	24.4	19.7	3.7	239	40.0	28.6	0.4	0.4	403	Cl–SO_4–HCO_3 Na–Mg–Ca
		5	July 07, 2020	8.5	+139.3	0	8.2	1.4	48	25.6	25.0	4.5	207	46.8	37.0	1.0	0.2	403	SO_4–Cl–HCO_3 Na–Mg–Ca
		6	May 12, 2019	8.7	+250.0	2	11.3	3.5	46	34.7	43.4	7.8	325	53.0	30.8	0.7	0.8	541	Cl–SO_4–HCO_3 Na–Ca–Mg
		6	July 08, 2020	8.7	+131.3	0	8.6	1.6	37	24.4	47.7	8.6	244	49.0	37.8	1.6	0.3	454	SO_4–Cl–HCO_3 Ca–Mg–Na
			Average:	**8.6**	**+192.6**	**1**	**8.7**	**2.2**	**45**	**27.3**	**33.9**	**6.1**	**254**	**47.2**	**33.5**	**0.9**	**0.4**	**450**	**–**
	rivers (group IV)	7	May 12, 2019	8.1	+247.3	–	10.1	3.7	81	32.7	41.2	3.9	386	80.0	21.4	3.5	3.7	650	SO_4–HCO_3 Na–Mg–Ca
		8	May 12, 2019	8.2	+260.5	1	11.4	3.9	84	32.4	42.9	4.9	442	83.0	23.1	1.2	3.0	712	SO_4–HCO_3 Na–Mg–Ca
		9	May 12, 2019	7.9	+210.0	3	6.9	5	86	27.6	35.1	3.8	420	77.0	15.2	1.2	3.0	665	SO_4–HCO_3 Na–Mg–Ca
		10	June 03, 2019	7.9	+231.0	4	1.7	4	74	43.0	37.0	1.5	470	26.2	21.0	0.8	1.6	672	HCO_3 Na–Mg–Ca
		11	June 03, 2019	7.9	+218.4	1	2.7	5.7	51	30.0	46.0	3.9	350	49.5	12.0	1.6	0,5	542	SO_4–HCO_3 Na–Mg–Ca
		12	June 03, 2019	8.1	+218.8	2	4.7	9.0	105	14.0	61.0	4.7	456	56.0	17.0	1.4	1,1	713	SO_4–HCO_3 Mg–Na–Ca
			Average:	**8.3**	**+215.6**	**1.4**	**7.2**	**4.0**	**66**	**28.8**	**39.9**	**4.7**	**354**	**56.0**	**24.4**	**1.3**	**1.5**	**575**	–

Note: dash means “no data”; PI* = permanganate index (oxygen demand), mg/L; **chemical types are presented according to the classification proposed by S. Shchukarev (the formula includes elements with contents above 10 %-equivalents). TDS – total dissolved solids.

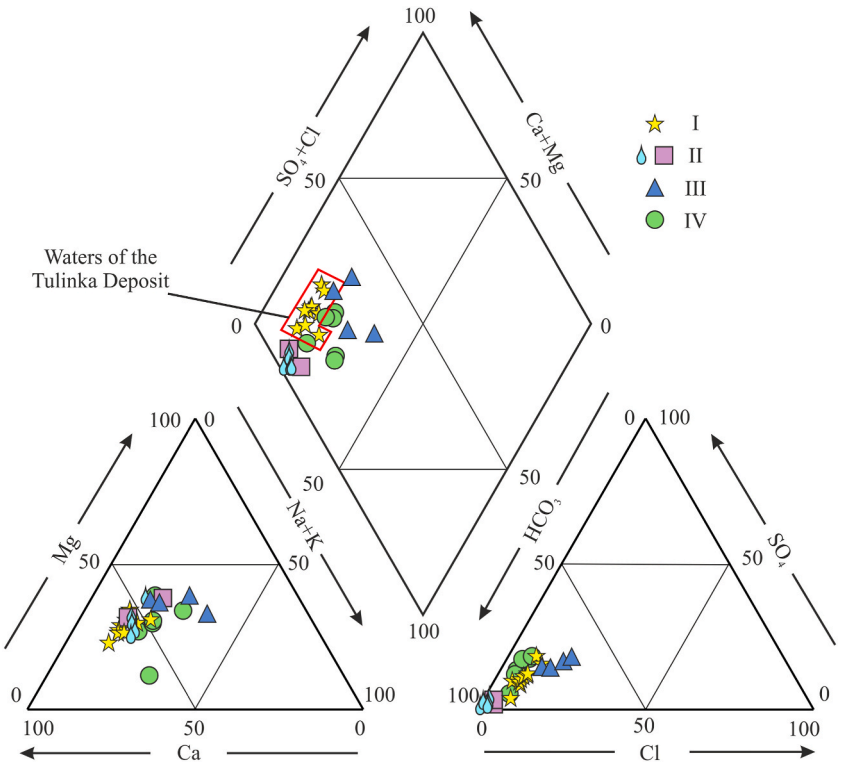

Fig. 3. Natural waters of the area in the Piper diagram. Group I - interstitial waters in sheared granitoids; group II - interstitial waters of regional fractured zone; group III - surface waters subject to anthropogenic effects, quarries; group IV - surface waters subject to anthropogenic effects, rivers.

chemistry of the four groups (Fig. 5): U concentrations are the highest in the Tulinka waters ($1.48 \bullet 10^{-2}$ to $1.73 \bullet 10^{-2}$ mg/L) and quite high in the flooded granite quarries ($9.80 \bullet 10^{-3}$ to $1.24 \bullet 10^{-2}$ mg/L). It should be stressed that the waters of the Upper Tula river contain $1.71 \bullet 10^{-2}$ mg/L U, approaching the concentration of uranium in radon-rich water (Table 2; Fig. 5), which requires further investigation.

4.3. Stable isotopes and DIC

Determination of stable isotopes ($\delta^{18}O$, δD and $\delta^{13}C$) and dissolved inorganic carbon (DIC) in groundwater has become indispensable in studies focused on the genesis of natural waters, connectivity of aquifers, rock-water interaction, and behavior of dissolved gases and organic carbon (Cartwright et al., 2000; Das et al., 2005; Soulsby et al., 2015; Chafouq et al., 2018; Hoefs, 2018; Boral et al., 2019; Santucci et al., 2019; Stefánsson et al., 2019; Yu et al., 2019; Aydin et al., 2020; Newman et al., 2020). Surface waters, as well as a large part of groundwaters, have meteoric sources (Boral et al., 2019; Cotovicz et al., 2019; Santucci et al., 2019; Wu et al., 2019; Aydin et al., 2020; Xia et al., 2020; Novikov et al., 2021b). The DIC and $\delta^{13}C_{DIC}$ patterns provide some evidence of the interaction of waters with host rocks (Zhang et al., 1995; Cartwright et al., 2000; Górka et al., 2011; Mickler et al., 2019; Novikov et al., 2021b) and, hence, of the availability, properties, and origin of carbon (atmospheric, organic, or biogenic CO_2, etc.).

The Tulinka waters show broad ranges of $\delta^{18}O$ and δD: 18.9 to −9.5‰ and −139.4 to −86.1‰, respectively (Table 3; Fig. 6). Most of the data plot along the global (Craig, 1961) and local (Novikov et al., 2022) meteoric water lines (GMWL and LMWL, respectively) and are thus of meteoric origin. However, some samples stand apart from the GMWL and LMWL trends (red ellipse in Fig. 6a) due to evaporation leading to heavier isotope values (Chafouq et al., 2018; Wu et al., 2019; Yu et al., 2019; Newman et al., 2020). The $\delta^{18}O$ shifts with respect to GMWL are listed in Table 3. The local evaporation line approaches the one reported previously (Novikov et al., 2022) for the northern Novosibirsk region, with the respective equations $y = 5.2x - 38.1$ and $y = 5.2x - 37.7$, where y is δD and x is $\delta^{18}O$.

The groundwater sampled from the Svyatoi spring, borehole 1 in Verkh Tula village, and the Tula river (site 10 in Fig. 1) have the most depleted hydrogen and oxygen isotope compositions: from −139.4 to −134.9‰ δD and −18.9 to −8.2‰ $\delta^{18}O$. Other Tula River samples (7, 8, 9 and 11 in Fig. 1) and those from the other borehole of Verkh Tula village show heavier isotope compositions of −131.1 to −122.6‰ δD and −16.9 to −16.2‰ $\delta^{18}O$. The average $\delta^{18}O$ and δD values in the Tulinka waters are still less negative (−15.3 and −113.7‰, respectively) and vary from −15.5 to −14.8‰ $\delta^{18}O$ and −114.2 to −112.8‰ δD, exhibiting seasonal variations. The samples from the shallow and slow Upper Tula river have the heaviest oxygen and hydrogen isotope compositions among the analyzed river waters (up to −13.2‰ $\delta^{18}O$ and −105.0‰ δD), due to greater evaporation (Novikov et al., 2020b), which led to a positive $\delta^{18}O$ shift of +1.2‰. The waters of the Gorsky and Tulinka flooded quarries differ from all other water samples by the least negative $\delta^{18}O$ and δD values (−12.4 and −9.5‰ $\delta^{18}O$; −103.2 and −86.1‰ δD, respectively) and the greatest $\delta^{18}O$ shifts of +1.8–2.6‰, which is the evidence of evaporation effect, most strongly pronounced in the quarries.

Thus, the oxygen and hydrogen isotope compositions of the Tulinka radon waters are heavier than in most of surface and ground (Svyatoi spring) waters. In the summer season, $\delta^{18}O$ and δD in groundwaters are commonly lighter than in surface waters, recharging mostly from rainfall and being subject to evapotranspiration. This pattern appears in the samples from the Svyatoi spring, which can be considered as background groundwaters in terms of oxygen and hydrogen isotope compositions.

Meanwhile, the $\delta^{18}O$ and δD values of the Tulinka samples, heavier than those of surface waters, provide implicit evidence that the aquifers feed from sources related neither to the rivers nor to the Svyatoi spring. Note that $\delta^{18}O$ and δD in the Tulinka waters, as well as in the Svyatoi spring, are poorly sensitive to seasonal effects and thus represent a zone of slow water exchange.

Dissolved carbon dioxide (DIC) in meteoric and surface waters most

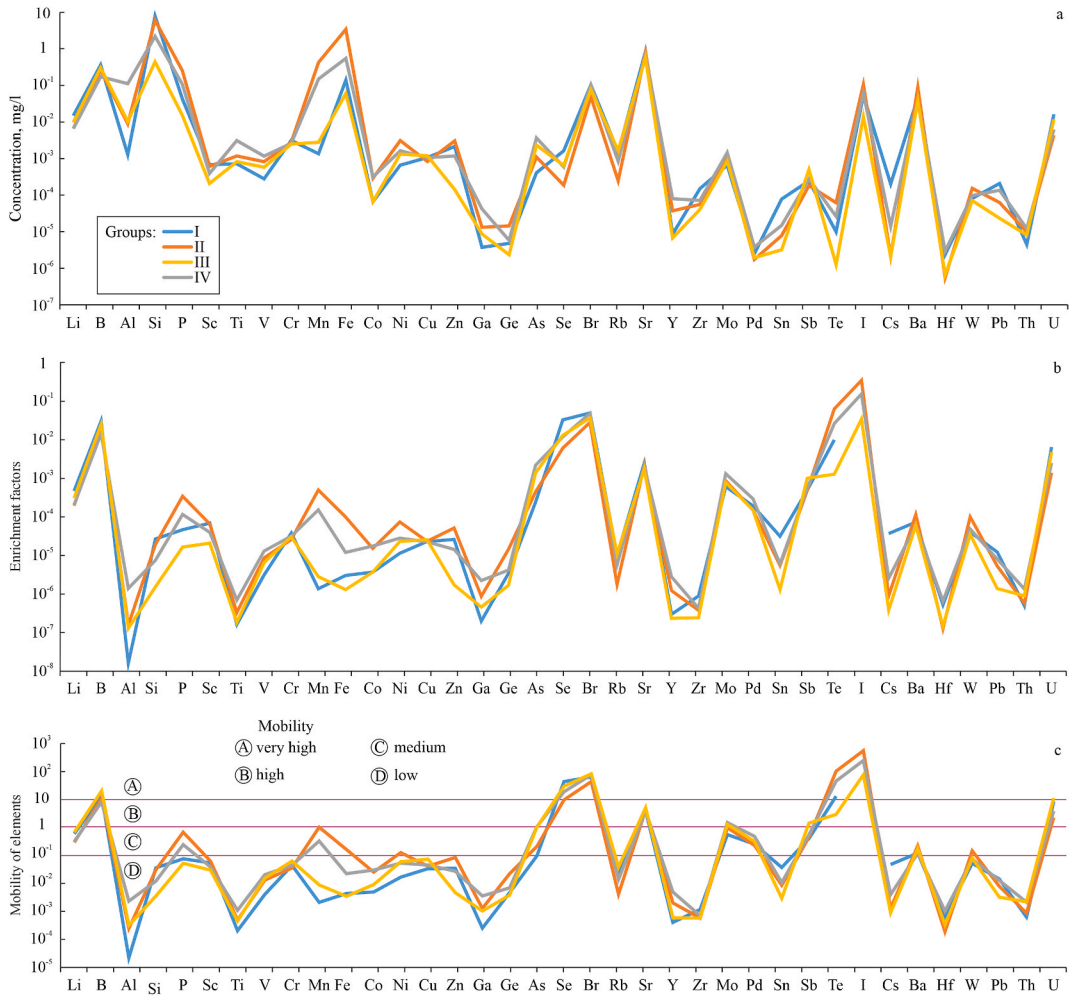

Fig. 4. Patterns of trace elements in the Tulinka radon waters (a), enrichment factors (b), and mobility of elements in natural waters (c). Group I - interstitial waters in sheared granitoids; group II - interstitial waters of regional fractured zone; group III - surface waters subject to anthropogenic effects, quarries; group IV - surface waters subject to anthropogenic effects, rivers.

likely originates from atmospheric CO_2. According to monitoring data for 2000–2020 and 2000–2010 reported from two nearest stations at Ulaan-Uul (Mongolia) and Sari Taukum (Kazakhstan), respectively (https://www.esrl.noaa.gov/gmd/dv/iadv/), $\delta^{13}C$ of atmospheric CO_2 varied from −7.5 to −9.3‰, with an average over 2019–2020 of −8.6‰, or from −8.0 to −7.8‰ (−7.9‰ on average) in the warm season. Capture of atmospheric CO_2 by meteoric waters and related fractionation upon the transition of gaseous to dissolved carbon dioxide ($CO_{2g} \rightarrow CO_{2aq}$) lead to 1.2‰ ^{13}C depletion of CO_2 (Zhang et al., 1995; Das et al., 2005). Therefore, mean annual $\delta^{13}C_{DIC}$ in meteoric waters is expected to be within −9.8‰ to −9.1‰, since dissolved CO_2 makes the greatest portion of DIC, while the background DIC concentration is $\sim 10^{-2}$ mmol/L (Das et al., 2005). In our case, however, DIC (a total of CO_{2aq}, CO_3^{2-}, and HCO_3^- components) is at least two orders of magnitude above this value (Table 3). Therefore, most of DIC at the Tulinka aquifers comes from soil CO_2 absorbed by infiltrating waters, rather than from atmospheric CO_2. The range of $\delta^{13}C_{DIC}$ in the analyzed samples (from −14.3 to −9.0‰) corresponds to a combined CO_2 origin: diffusion of soil CO_2 approaching the atmospheric $\delta^{13}C_{CO2}$ values, and biogenic CO_2 released by decaying plant residues, which then participates in mixed silicate-carbonate weathering (Das et al., 2005).

The $\delta^{13}C_{DIC}$ values of the Tulinka waters varied with time in the course of monitoring, from May 2019 through March 2020 (Fig. 6b), with a peak of the heaviest $\delta^{13}C_{DIC}$ (−9.9‰) in August–September 2019. After the peak, the curve descends gradually and returns to the $\delta^{13}C_{DIC}$ values of mid-2019 b y March 2020. This pattern may result from the transport of biogenic CO_2 through soil to the Tulinka aquifers with spring flood and meteoric waters. Indeed, the $\delta^{13}C_{DIC}$ peak, which corresponds to the smallest contribution of biogenic CO_2 into $\delta^{13}C$ of soil carbon dioxide, falls at the beginning of the driest season, when the spring floods and the related voluminous water infiltration through soil already ceases, while the meteoric activity does not start yet (without regard to additional insolation and evaporation effects). Thus, this is a period of the lowest infiltration, when only small amounts of meteoric waters can transport soil CO_2, like a chromatographic eluent, to aquifers (ultimate consumers).

Heavy rainfalls since late August till early November provide new inputs of soil CO_2 enriched in the isotopically light biogenic component into groundwaters. The process is inertial and occurs concurrently with soil freezing, which hinders the migration of biogenic CO_2. This may be the cause of the plateau on the curve between November and February 2020 (Fig. 6b). The transport of biogenic soil CO_2 to groundwaters and ^{12}C enrichment of dissolved carbon dioxide resume in the season of snow melting and spring floods.

The DIC concentration in the Tulinka waters varied only slightly over the year-long observation period (from 5300 to 6200 μmol/L), i.e., the changes in CO_2 inputs were minor. The observed $\delta^{13}C_{DIC}$ variations require dramatically different $\delta^{13}C$ of the carbon dioxide transported by this mechanism (as in the case of biogenic CO_2).

Inorganic carbon dissolved in the waters of the Tulinka aquifers and

Table 2
Element ratios and radionuclides in natural waters.

No in Fig. 1	Sampling date	Ca/Na	Ca/Mg	Ca/Si	Mg/Si	Na/Si	Si/Na	rNa/rCl	SO_4/Cl	^{222}Rn, *	^{232}Th, *	^{238}U, *	^{232}Th/^{238}U
Interstitial waters in sheared granitoids (group I)													
1	May 13, 2019	3.83	3.48	16.34	4.69	4.26	0.23	1.77	2.09	–	$1.10\bullet10^{-5}$	$1.68\bullet10^{-2}$	$6.55\bullet10^{-4}$
1	May 30, 2019	2.00	2.45	17.47	7.15	8.75	0.11	2.40	1.44	173.0	$2.63\bullet10^{-6}$	$1.68\bullet10^{-2}$	$1.56\bullet10^{-4}$
1	June 27, 2019	4.52	4.42	21.80	4.93	4.82	0.21	1.80	1.93	218.0	bd	$1.73\bullet10^{-2}$	–
1	August 01, 2019	3.19	2.87	13.77	4.79	4.31	0.23	1.17	3.21	–	$1.58\bullet10^{-5}$	$1.67\bullet10^{-2}$	$9.42\bullet10^{-4}$
1	September 03, 2019	3.47	3.48	14.07	4.04	4.06	0.25	1.73	2.63	247.0	$9.59\bullet10^{-7}$	$1.65\bullet10^{-2}$	$5.81\bullet10^{-5}$
1	October 09, 2019	4.52	4.42	22.84	5.17	5.05	0.20	1.17	1.93	–	bd	$1.51\bullet10^{-2}$	–
1	November 12, 2019	3.85	3.20	16.19	5.06	4.20	0.24	1.09	0.85	218.0	$3.45\bullet10^{-6}$	$1.48\bullet10^{-2}$	$2.33\bullet10^{-4}$
1	December 11, 2019	3.57	2.88	14.03	4.88	3.93	0.25	1.11	1.98	217.0	bd	$1.49\bullet10^{-2}$	–
1	January 21, 2020	3.82	3.55	15.76	4.44	4.12	0.24	1.17	2.10	–	bd	$1.57\bullet10^{-2}$	–
1	February 12, 2020	3.61	2.39	12.65	5.29	3.51	0.29	0.80	1.96	–	bd	$1.53\bullet10^{-2}$	–
1	March 18, 2020	2.68	2.82	11.86	4.21	4.44	0.23	1.34	1.98	276.0	$1.75\bullet10^{-6}$	$1.56\bullet10^{-2}$	$1.13\bullet10^{-4}$
Average:		**3.55**	**3.27**	**16.07**	**4.97**	**4.68**	**0.23**	**1.41**	**2.01**	**225.0**	$\mathbf{5.93\bullet10^{-6}}$	$\mathbf{1.60\bullet10^{-2}}$	$\mathbf{3.60\bullet10^{-4}}$
Interstitial waters in regional fractured zone (group II)													
2	June 17, 2019	1.70	1.69	11.60	6.87	6.84	0.15	7.16	2.04	6.0	$7.00\bullet10^{-6}$	$3.80\bullet10^{-6}$	1.84
3	June 17, 2019	3.31	2.75	16.02	5.83	4.84	0.21	3.72	0.95	0.0	$8.00\bullet10^{-6}$	$2.70\bullet10^{-6}$	2.96
4	June 03, 2019	2.51	1.90	19.66	10.32	7.83	0.13	4.42	1.65	28.0	$8.00\bullet10^{-6}$	$5.30\bullet10^{-3}$	$1.51\bullet10^{-3}$
4	June 27, 2019	2.96	2.91	12.08	4.15	4.08	0.25	24.56	4.55	16.0	bd	$7.10\bullet10^{-3}$	–
4	February 24, 2020	3.17	2.63	22.26	8.48	7.02	0.14	5.60	3.70	10.0	$3.01\bullet10^{-7}$	$4.73\bullet10^{-3}$	$6.38\bullet10^{-5}$
4	June 23, 2020	2.77	3.56	14.40	4.04	5.19	0.19	49.52	13.24	17.0	$2.41\bullet10^{-5}$	$5.62\bullet10^{-3}$	$4.29\bullet10^{-3}$
4	July 07, 2020	2.63	3.21	12.78	3.98	4.86	0.21	7.48	1.10	11.0	$1.76\bullet10^{-5}$	$7.26\bullet10^{-3}$	$2.42\bullet10^{-3}$
Average:		**2,72**	**2.66**	**15.54**	**6.24**	**5.81**	**0.18**	**14.64**	**3.89**	**12.6**	$\mathbf{1.08\bullet10^{-5}}$	$\mathbf{4.29\bullet10^{-3}}$	**0.80**
Surface water subject to anthropogenic effects, quarries (group III)													
5	May 12, 2019	2.42	1.95	119.00	61.00	49.25	0.02	1.06	1.40	0.3	$1.00\bullet10^{-5}$	$9.80\bullet10^{-3}$	$1,02\bullet10^{-3}$
5	July 07, 2020	1.07	1.34	59.49	44.49	55.64	0.02	2.17	1.72	0.1	$1.15\bullet10^{-5}$	$1.24\bullet10^{-2}$	$9,30\bullet10^{-4}$
6	May 12, 2019	1.92	1.87	190.66	101.77	99.38	0.01	0.99	1.26	2.0	$3.20\bullet10^{-6}$	$1.21\bullet10^{-2}$	$2,64\bullet10^{-4}$
6	July 08, 2020	0.78	1.52	117.29	77.34	151.25	0.01	1.93	1.30	0.2	$7.08\bullet10^{-6}$	$1.23\bullet10^{-2}$	$5,77\bullet10^{-4}$
Average:		**1,55**	**1.67**	**121.61**	**71.15**	**88.88**	**0.02**	**1.54**	**1.42**	**0.65**	$\mathbf{7.96\bullet10^{-6}}$	$\mathbf{1.16\bullet10^{-2}}$	$\mathbf{6.98\bullet10^{-4}}$
Surface water subject to anthropogenic effects, rivers (group IV)													
7	May 12, 2019	1.97	2.48	21.66	8.74	11.02	0.09	2.97	3.74	0.1	$5.40\bullet10^{-6}$	$4.80\bullet10^{-3}$	$1,13\bullet10^{-3}$
8	May 12, 2019	1.96	2.59	27.63	10.66	14.11	0.07	2.86	3.59	1.0	$5.00\bullet10^{-7}$	$4.80\bullet10^{-3}$	$1,04\bullet10^{-4}$
9	May 12, 2019	2.46	3.13	28.80	9.20	11.71	0.09	3.56	5.07	3.0	bd	$4.60\bullet10^{-3}$	–
10	June 03, 2019	2.00	1.73	47.13	27.20	23.57	0.04	2.72	1.25	4.0	$2.37\bullet10^{-5}$	$1.60\bullet10^{-3}$	$1,48\bullet10^{-2}$
11	June 03, 2019	1.11	1.70	110.87	65.22	100.00	0.01	5.91	4.13	1.0	$1.50\bullet10^{-5}$	$3.90\bullet10^{-3}$	$3,85\bullet10^{-3}$
12	June 03, 2019	1.73	7.55	96.33	12.75	55.64	0.02	5.50	3.29	2.0	$2.44\bullet10^{-5}$	$1.71\bullet10^{-2}$	$1,43\bullet10^{-3}$
Average:		**1,87**	**3.20**	**55.40**	**22.30**	**36.01**	**0.05**	**3.92**	**3.51**	**1.85**	$\mathbf{1.38\bullet10^{-5}}$	$\mathbf{6.13\bullet10^{-3}}$	$\mathbf{4.26\bullet10^{-3}}$

Note: dash means "no data"; bd = below detection limit; * = concentration, mg/L.

the Svyatoi spring has radiocarbon ages of 2663 ± 144 and 4518 ± 93 years, respectively, and is thus of ancient origin. However, the obtained ^{14}C dates are only approximate as they do not take into account such factors as sources of DIC in the waters, distribution of carbon species in ambient gases and rocks, leaching from rocks, etc. (Stefánsson et al., 2019), which should be a subject of a separate study. Nevertheless, our results provide further evidence for water circulation through different aquifers: surface waters carrying modern dissolved carbon coexist with at least two sites of ancient carbon.

The younger age of DIC in the Tulinka waters relative to that in the Svyatoi spring may be due to inputs of modern soil CO_2 and to flooding. However, the contribution of modern CO_2 must be rather small, as suggested by minor DIC variations over the year (see above). Anyway, the age of the Tulinka waters is only tentative.

5. Conclusions

The radon-laden waters of the Tulinka aquifers (Table 1) have SO_4–HCO_3 Na–Mg–Ca major-ion chemistry, with TDS 720–910 mg/L and Si content 6.41–9.02 mg/L. The variables (pH, Eh and the concentration of dissolved O_2) are mainly controlled by local geology and water exchange patterns. The Tulinka waters have neutral to slightly alkaline pH (7.3–7.7) and Eh values corresponding to the oxidized environment (+169.1 to +250.0 mV), and contain 2.86–7.37 mg/L of dissolved oxygen.

The results obtained in the studies allow us to conclude that:

1. Radon-rich groundwaters in the Tulinka area occur in two aquifers. They are (i) pore waters in Quaternary sediments (a_3Q_{IV} alluvium and the Krasnaya Dubrovka (L,laI-IIkd) and Kochkovo (a,lE$_2$kč) Formations); (ii) interstitial waters in sheared granites of the Novosibirsk complex (the main phase). The Tulinka radon-rich waters in both aquifers are affected by anthropogenic pollution as a result of flooding.
2. According to the composition signatures of the Tulinka waters, in particular, significant concentration of nitrates, 30.0–59.3 mg/L, and element ratios Ca/Na = 3.5, Ca/Mg = 3.3, Ca/Si = 16.1, Mg/Si = 5.0, Na/Si = 4.7, Si/Na = 0.2, rNa/rCl = 1.4, and SO_4/Cl = 2.0, these are interstitial waters in sheared granites.
3. The radon activity in the Tulinka waters varies from 160 to 276 Bq/L ^{222}Rn, and the concentrations of U, Th, and Ra isotopes are 0.015–0.017 mg/L ^{238}U, $9.59\bullet10^{-7}$ to $1.58\bullet10^{-5}$ mg/L ^{232}Th, and up to $4.93\bullet10^{-10}$ mg/L ^{226}Ra. The ^{232}Th/^{238}U ratio ranges from $5.81\bullet10^{-5}$ to $9.42\bullet10^{-4}$. The total ά activity is not higher than 891 mBq/L, and β-activity is 80 mBq/L. The activity values for U and Ra isotopes are 706 mBq/L for ^{234}U, 196 mBq/L for ^{238}U, 18 mBq/L for ^{226}Ra, and 20 mBq/L for ^{228}Ra. The ^{234}U/^{238}U ratio (γ) does not exceed 3.6.
4. The measured isotope characteristics provide evidence in favor of the meteoric origin of the Tulinka waters, recharging by infiltration. The ranges of stable isotopes are within −15.4 to −15.1‰ δ^{18}O, −114.2 to −112.8‰ δD, and −13.9 to −9.9‰ $\delta^{13}C_{DIC}$. The recharge patterns of the waters are independent of seasonal climate variations, which is a sign of the zone of slow water exchange.
5. The $\delta^{13}C_{DIC}$ values vary with time, presumably in yearly cycles, and reach a peak in August–September. The range of $\delta^{13}C_{DIC}$ in the analyzed samples (from −14.3 to −9.0‰) corresponds to a combined CO_2 origin: diffusion of soil CO_2 approaching the atmospheric

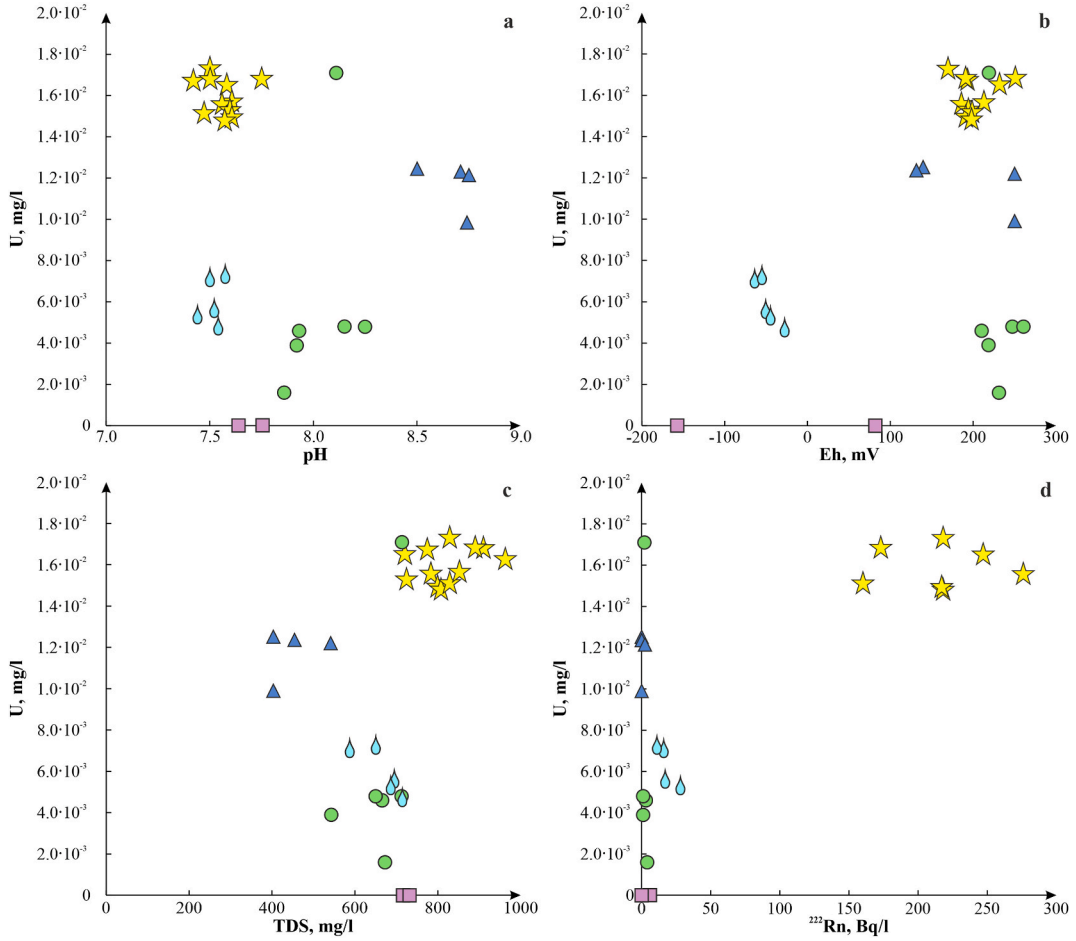

Fig. 5. Uranium concentration vs. different variables: pH (a), Eh (b), TDS (c), radon activity (d). Points relate to sampling sites as designated in Fig. 1.

Table 3
Isotope systematics and DIC of natural waters.

No in Fig. 1	Sampling date	HCO_3^-, μmol/L	$\delta^{13}C_{VPDB}$, ‰	$\Delta\delta^{13}C_{DIC}$, ‰	$\delta\ D_{VSMOW}$, ‰	ΔδD, ‰	$\delta\ ^{18}O_{VSMOW}$, ‰	$\Delta\delta^{18}O$, ‰	$\delta^{18}O$ shift
1	May 13, 2019	6172	−13.2	0.1	−113.7	1.0	−15.4	0.1	0.1
1	May 30, 2019	6736	−13.1	0.0	−114.2	0.4	−15.2	0.3	0.3
1	June 27, 2019	6092	−12.5	0.1	−113.6	0.1	−15.3	0.3	0.1
1	August 01, 2019	5287	−13.3	0.1	−112.8	0.5	−15.1	0.1	0.3
1	September 03, 2019	5540	−9.9	0.2	−113.7	0.8	−15.2	0.1	0.3
1	October 09, 2019	6092	−10.8	0.2	−113.8	1.4	−15.3	0.1	0.2
1	November 12, 2019	6448	−11.3	0.2	−114.2	0.3	−15.2	0.1	0.3
1	December 11, 2019	6000	−12.0	0.0	−112.9	0.1	−15.3	0.1	0.1
1	January 21, 2020	5747	−11.9	0.1	−114.1	1.1	−15.5	0.1	0.0
1	February 12, 2020	4517	−12.5	0.1	−113.8	1.8	−14.8	0.2	0.6
1	March 18, 2020	5218	−13.9	0.1	−113.1	1.0	−15.4	0.1	0.0
2	June 17, 2019	6149	−14.2	0.1	−136.3	0.3	−18.3	0.0	−0.1
3	June 17, 2019	6034	−14.3	0.2	−122.6	0.2	−16.5	0.4	0.1
4	June 03, 2019	5885	−14.0	0.1	−139.4	1.8	−18.9	0.4	−0.2
4	June 27, 2019	5115	−12.8	0.0	−136.8	0.7	−18.3	0.3	0.1
4	November 03, 2019	–	−12.9	0.1	−136.3	0.3	−18.4	0.1	−0.1
4	February 24, 2020	5977	−13.2	0.1	−138.5	0.4	−18.2	0.1	0.4
4	July 07, 2020	5402	−12.8	0.2	−137.5	1.3	−18.8	0.0	0.5
5	May 12, 2019	2747	−9.4	0.0	−103.2	1.1	−12.4	0.2	1.8
5	July 07, 2020	2379	−10.0	0.1	−116.6	1.4	−15.3	0.2	0.5
6	May 12, 2019	3736	−9.0	0.0	−86.1	0.3	−9.5	0.1	2.6
6	July 08, 2020	2805	−12.6	0.2	−124.5	0.2	−16.2	0.1	0.6
7	May 12, 2019	4437	−12.9	0.0	−124.7	1.0	−16.2	0.3	0.7
8	May 12, 2019	5080	−12.5	0.0	−128.1	2.0	−16.8	0.3	0.4
9	May 12, 2019	4828	−12.6	0.2	−131.1	−1.0	−16.9	0.2	0.7
10	June 03, 2019	5402	−12.6	0.1	−134.9	1.5	−18.3	0.4	−0.1
11	June 03, 2019	4023	−12.5	0.1	−125.7	0.8	−16.3	0.3	0.6
12	June 03, 2019	5241	−14.1	0.1	−105.0	1.3	−13.2	0.3	1.2

Note. Subscripts VPDB and VSMOW mean that the corresponding values are given with respect to the Standard Isotope Samples: Vienna PeeDee Belemnite and Vienna Standard Mean Ocean Water, respectively.

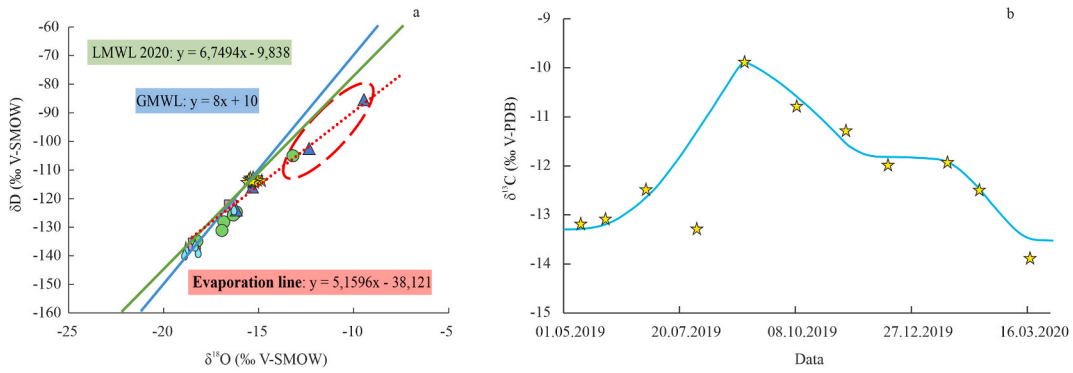

Fig. 6. Patterns of stable isotopes in the Tulinka radon waters: δD vs. δ18 (a), time-dependent δ13CDIC in May 2019 through March 2020 (b).

$\delta^{13}C_{CO2}$ values, and biogenic CO_2 released by decaying plant residues.

6. For the first time, dissolved inorganic carbon was dated by means of the radiocarbon method as 2663 ± 144 years in the Tulinka waters and 4518 ± 93 years in the Svyatoi spring. However, the ^{14}C ages are most likely underestimated, because the groundwaters are mixed with infiltrated modern surface waters.

Declaration of competing interest

The authors declare that they have no known competing financial interests or personal relationships that could have appeared to influence the work reported in this paper.

Data availability

Data will be made available on request.

Acknowledgments

The field and analytical work on chemistry of natural waters was supported by the Ministry of Science and Higher Education of the Russian Federation (Projects FSWW-0022-0014 and FSWW-0022-2020). The analytical work on determination of stable isotopes and dissolved inorganic carbon was supported by the Russian Science Foundation and government of Novosibirsk Oblast (Project 22-17-20029).

Authors thank analysts from the Tomsk National Research Polytechnical University O.V. Chebotareva, N.V. Bubliy, A.S. Pogutsa, V.V. Kurovskaya, K.B. Krivtsova, and L.A. Rakul for having carried out the analytical work for the present study.

References

Abu-Khader, M.M., Shawaqfeh, A.T., Naddaf, Z., Maity, J.P., Bhattacharya, P., 2018. Radon in the groundwater in the Amman-Zarqa Basin and related environments in Jordan. Groundwater Sustain. Dev. 7, 73–81.

Atkins, M.L., Santos, I.R., Perkins, A., Maher, D.T., 2016. Dissolved radon and uranium in groundwater in a potential coal seam gas development region (Richmond River Catchment, Australia). J. Environ. Radioact. 154, 83–92.

Aydin, H., Karakuş, H., Mutlu, H., 2020. Hydrogeochemistry of geothermal waters in eastern Turkey: Geochemical and isotopic constraints on water-rock interaction. J. Volcanol. Geoth. Res. 390, 106708.

Babin, G.A., Chernykh, A.I., Golovina, A.G., Zhigalov, S.V., Dolgushin, S.S., Vetrov, E.V., Corableva, T.V., Bodina, N.A., Svetlova, N.A., Fedoseev, G.S., Khilko, A.P., Epifanov, V.A., Loskutov, YuI., Loskutov, I.Yu, Mikharevich, M.V., Pihutin, E.A., 2015. Geological Map of the Russian Federation. Scale 1 : 1 000 000 (Third Generation). Series Altai-Sayan. Sheet N-44, Novosibirsk. Explanatory Note. Kartfabrika VSEGEI, St. Petersburg, 392 pp. (in Russian).

Beitollahi, M., Ghiassi-Nejad, M., Esmaeli, A., Dunker, R., 2007. Radiological studies in the hot spring region of Mahallat, central Iran. Radiat. Protect. Dosim. 123 (4), 505–508.

Bertolo, A., Bigliotto, C., 2004. Radon concentration in waters of geothermal Euganean basin-Veneto, Italy. Radiat. Prot. Dosimetry 111 (4), 355–358.

Bohm, C., 2002. Radon in Wasser-Uberblick für den Kanton Graubünden. NGG Jahresberichte 111, 49–79.

Boral, S., Sen, I.S., Ghosal, D., Peucker-Ehrenbrink, B., Hemingway, J.D., 2019. Stable water isotope modeling reveals spatio-temporal variability of glacier meltwater contributions to Ganges River headwaters. J. Hydrol 577, 123983.

Cartwright, I., Weaver, T., Tweed, S., Ahearne, D., Cooper, M., Czapnik, C., Tranter, J., 2000. O, H, C isotope geochemistry of carbonated mineral springs in central Victoria, Australia: sources of gas and water–rock interaction during dying basaltic volcanism. J. Geochem. Explor. 257 (26), 69–70.

Chafouq, D., Mandour, A.El, Elgettafi, M., Himi, M., Chouikri, I., Casas, A., 2018. Hydrochemical and isotopic characterization of groundwater in the Ghis-Nekor plain (northern Morocco). J. Afr. Earth Sci. 139, 1–13.

Cotovicz Jr., L.C., Knoppers, B.A., Deirmendjian, L., Abril, G., 2019. Sources and sinks of dissolved inorganic carbon in an urban tropical coastal bay revealed by $\delta^{13}C$-DIC signals. Estuar. Coast Shelf Sci. 220, 185–195.

Craig, H., 1961. Isotopic variations in meteoric waters. Science 133, 1702–1703.

Das, A., Krishnaswami, S., Bhattacharya, S.K., 2005. Carbon isotope ratio of dissolved inorganic carbon (DIC) in rivers draining the Deccan Traps, India: Sources of DIC and their magnitudes. Earth Planet Sci. Lett. 236 (1–2), 419–429.

Duenas, C., Fernandez, M.C., Enrıquez, C., Carretero, J., Liger, E., 1998. Natural radioactivity levels in Andalusian spas. Water Res. 32 (8), 2271–2278.

Epstein, S., Mayeda, T., 1953. Variation of ^{18}O content of waters from natural sources. Geochem. Cosmochim. Acta 4 (5), 213–224, 2.

Evans, M.J., Derry, L.A., France-Lanord, C., 2008. Degassing of metamorphic carbon dioxide from the Nepal Himalaya. G-cubed 9 (4), 1–18.

Górka, M., Sauer, P.E., Lewicka-Szczebak, D., Jędrysek, M.O., 2011. Carbon isotope signature of dissolved inorganic carbon (DIC) in precipitation and atmospheric CO_2. Environ. Pollut. 159 (1), 294–301.

Gurler, O., Akar, U., Kahraman, A., 2010. Measurements of radon levels in thermal waters of Bursa, Turkey. Fresenius Environ. Bull. 19 (12), 3013–3017.

Hoefs, J., 2018. Stable isotope geochemistry. In: Springer Textbooks in Earth Sciences, Geography and Environment. Springer Inter. Publ. AG, part of Springer Nature, eighth ed., p. 460.

Horvath, A.D., Bohus, L.O., Urbani, F., Marx, G., Piroth, A., Greaves, E.D., 2000. Radon concentrations in hot spring waters in northern Venezuela. J. Environ. Radioact. 47 (2), 127–133. https://www.esrl.noaa.gov/gmd/dv/iadv/. last visited: 5.11.2020.

Kopec, B.G., Feng, X., Posmentier, E.S., Sonder, L.J., 2019. Seasonal deuterium excess variations of precipitation at Summit, Greenland, and their climatological significance. J. Geophys. Res. Atmospheres 124, 72–91.

Mickler, P.J., Carlson, P., Banner, J.L., Breecker, D.O., Stern, L., Guilfoyle, A., 2019. Quantifying carbon isotope disequilibrium during in-cave evolution of drip water along discreet flow paths. Geochem. Cosmochim. Acta 244, 182–196.

Mittal, S., Rani, A., Mehra, R., 2016. Radon levels in drinking water and soil samples of Jodhpur and Nagaur districts of Rajasthan, India. Appl. Radiat. Isot. 113, 53–59.

Nelson, S.T., 2000. A simple, practical methodology for routine VSMOW/SLAP normalization of water samples analysed by continuous flow methods. Rapid Commun. Mass Spectrom. 14, 1044–1046.

Newman, C.P., Poulson, S.R., Hanna, B., 2020. Regional isotopic investigation of evaporation and water-rock interaction in mine pit lakes in Nevada, USA. J. Geochem. Explor. 210, 15, 106445.

Nikolov, J., Todorovic, N., Petrovic Pantic, T., Forkapic, S., Mrdja, D., Bikit, I., Krmar, M., Veskovic, M., 2012. Exposure to radon in the radon spa Niska Banja, Serbia. Radiat. Meas. 47, 443–450.

Novikov, D.A., Dultsev, F.F., Chernykh, A.V., 2020a. Role of water-rock interactions in the formation of the composition of radon waters of the Zaeltsovsky field (the southern part of West Siberia). J. Phys.: Conf. Ser 1451, 5, 012007.

Novikov, D.A., Dultsev, F.F., Maksimova, A.A., Pyryaev, A.N., Fage, A.N., Khvashchevskaya, A.A., Derkachev, A.S., Chernykh, A.V., 2022. Initial results of the integrated isotope-hydrogeochemical studies of the Novobibeevo occurrence of radon-rich waters. Bull. Tomsk Polytech. Univ., Geo. Assets Eng. 333 (1), 57–72.

Novikov, D.A., Korneeva, T.V., 2019. Microelements in radon waters of the Zaeltsovsky field (the southern part of West Siberia). J. Phys. Conf. Ser 1172, 6, 012096.

Novikov, D.A., Maksimova, A.A., Pyrayev, A.N., Yan, P.A., 2020b. First isotope-hydrogeochemical data on the natural waters of the south-east slope of the Chekanovsky ridge (Arctic areas of the Siberian Platform). Bull. Tomsk Polytech. Univ., Geo. Assets Eng. 331 (11), 157–167.

Novikov, D.A., Pyrayev, A.N., Chernykh, A.V., Dultsev, F.F., Ilyin, A.V., Chertovskikh, E. O., 2021b. New data on the isotopic composition ($\delta^{13}C$, δD, $\delta^{18}O$, $^{87}Rb/^{86}Sr$ and $^{87}Sr/^{86}Sr$) of the Siberian platform brines. Bull. Tomsk Polytech. Univ., Geo. Assets Eng. 332 (7), 20–33.

Novikov, D.A., Sukhorukova, A.F., Korneeva, T.V., 2018. Hydrogeology and water chemistry of the Zaeltsovsky-Mochishche occurrence of radon-laden waters (southern West Siberia). Geodyn. Tectonophys. 9 (4), 1255–1274.

Novikov, D.A., Sukhorukova, A.F., Korneeva, T.V., Kamenova-Totseva, R.M., Maksimova, A.A., Derkachev, A.S., Dultsev, F.F., Chernykkh, A.V., 2021a. Hydrogeology and water chemistry of the Kamenka field of radon waters (Novosibirsk). Bull. Tomsk Polytech. Univ., Eng. Georesour. 332 (4), 192–208.

Osmond, J.K., Rydell, H.S., 1968. Kaufman M. I. Uranium disequilibrium in groundwater: Anisotope dilution approach in hydrologic investigations. Science 162 (3857), 997–999.

Poojitha, C.G., Sahoo, B.K., Ganesh, K.E., Pranesha, T.S., Sapra, B.K., 2020. Assessment of radon and thoron exhalation from soils and dissolved radon in ground water in the vicinity of elevated granitic hill, Chikkaballapur district, Karnataka, India. Radiat. Protect. Dosim. 190 (2), 185–192.

Posokhov, E.V., Tolstikhin, N.I., 1977. Mineral Waters for Health Care, Industry, and Power Engineering, vol. 240. Nedra, Leningrad (in Russian).

Roba, C.A., Nita, D., Cosma, C., Codrea, V., Olah, S., 2012. Correlations between radium and radon occurrence and hydrogeochemical features for various geothermal aquifers in northwestern Romania. Geothermics 42, 32–46.

Santucci, L., Sanci, R., Carol, E., Villalba, E., Panarello, H., 2019. Using H, O, Rn isotopes and hydrometric parameters to assess the surface water-groundwater interaction in coastal wetlands associated to the marginal forest of the Río de la Plata. Continent. Shelf Res. 186, 104–110.

Scientific Council on Analytical Methods (SCAM), 1987. Groundwaters. Intralaboratory control of the quality of analyses carried out at the laboratories of the Ministry of Geology of the USSR. Moscow Times (In Russ.).

Seminsky, K.Zh, Burzunova, YuP., Seminsky, A.K., Bobrov, A.A., 2017. Role of the structural factor in the distribution of high-radon groundwater in the southwestern flank of the South Baikal rift basin. Geodyn. Tectonophys. 8 (4), 949–969.

Song, G., Wang, X., Chen, D., Chen, Y., 2011. Contribution of ^{222}Rn bearing water to indoor radon and indoor air quality assessment in hot spring hotels of Guangdong, China. J. Environ. Radioact. 102 (4), 400–406.

Soulsby, C., Birkel, C., Geris, J., Dick, J., Tunaley, C., Tetzlaff, D., 2015. Stream water age distributions controlled by storage dynamics and nonlinear hydrologic connectivity: modeling with high-resolution isotope data. Water Resour. Res. 51, 7759–7776.

Standard, State, 2020. Natural mineral drinking waters. General technical conditions. Working Document GOST 54316–2020. In: System of Standards on Information, Libraries, and Publishing, Standartinform, Moscow (in Russian).

Stefánsson, A., Arnorsson, S., Sveinbjörnsdóttir, A.E., Heinemaier, J., 2019. Isotope (δD, $\delta^{18}O$, ^{3}H, $\delta^{13}C$, ^{14}C) and chemical (B, Cl) constrains on water origin, mixing, water-rock interaction and age of low-temperature geothermal water. J. Appl. Geochem 108, 104380.

Telahigue, F., Agoubi, B., Souid, F., Kharroubi, A., 2018. Groundwater chemistry and radon-222 distribution in Jerba Island, Tunisia. J. Environ. Radioact. 182, 74–84.

Wu, H., Wu, J., Song, F., Abuduwaili, J., Saparov, A.S., Chen, X., Shen, B., 2019. Spatial distribution and controlling factors of surface water stable isotope values ($\delta^{18}O$ and $\delta^{2}H$) across Kazakhstan. Central Asia. Sci. Total Environ 678, 53–61.

Xia, Z., Zheng, Y., Stelling, J.M., Loisel, J., Huang, Y., Yu, Z., 2020. Environmental controls on the carbon and water (H and O) isotopes in peatland Sphagnum mosses. Geochem. Cosmochim. Acta 277, 265–284.

Yu, H., Ma, T., Du, Y., Chen, L., 2019. Genesis of formation water in the northern sedimentary basin of South China Sea: Clues from hydrochemistry and stable isotopes (D, ^{18}O, ^{37}Cl and ^{81}Br. J. Geochem. Explor. 196, 57–65.

Zhang, J., Quay, P.D., Wilbur, D.O., 1995. Carbon isotope fractionation during gas-water exchange and dissolution of CO_2. Geochem. Cosmochim. Acta 59 (1), 107–114.